C. R. Mecanique 338 (2010) 85–96

Contents lists available at ScienceDirect

Comptes Rendus Mecanique

www.sciencedirect.com

Aptitude of a lattice Boltzmann method for evaluating transitional thresholds for low Prandtl number flows in enclosures

Aptitude d'une méthode de type gaz sur réseau pour les écoulements à brisure de symétrie

Mohammed El Ganaoui *, R. Djebali

Université de Limoges/CNRS, faculté des sciences et techniques, 123, avenue Albert-Thomas, 87060 Limoges, France

ARTICLE INFO

Article history:
Received 25 March 2009
Accepted after revision 16 December 2009

Presented by Michel Combarnous

Keywords:
Continuum mechanics
Symmetry breaking
Lattice Boltzmann

Mots-clés :
Milieux continus
Brisure de symétrie
Gaz sur réseau

ABSTRACT

Lattice Boltzmann (LB) method is considered versus classical discretisation approaches to solve the problem of heat and fluid flow. The work considers situations with symmetry breaking for low Prandtl number fluids flowing in enclosures interesting directional solidification industry. The computed results demonstrate a good LB method's ability to captivate flow bifurcation thresholds. Particularly cavities exhibiting bifurcation sequences are considered and results are consistent with prior observations.

RÉSUMÉ

L'approche gaz sur réseaux est comparée aux méthodes de discrétisation classiques pour résoudre le problème de transferts de chaleur et d'écoulement. Le travail considère des situations de faible nombre de Prandtl avec brisure de symétrie dans des cavités intéressant des configurations de solidification dirigée. Les résultats illustrent un bon accord avec les scénarios existants dans le cas d'écoulements avec bifurcation.

Version française abrégée

Les méthodes dites de gaz sur réseau (Lattice Boltzmann) s'imposent progressivement comme une alternative sérieuse aux méthodes traditionnelles pour la mécanique numérique des fluides. Il s'agit d'une classe d'approches pour particules mesoscopiques pour simuler les mouvements de fluides et sont particulièrement adaptées pour modéliser des écoulements autour d'obstacles et facilement mises en œuvre sur machines parallèles [1–11].

En gaz sur réseau, les particules occupent les noeuds d'un réseau discret et transitent d'un nœud au prochain dans une phase de propagation. Puis, les particules se heurtent et obtiennent une nouvelle vitesse. C'est la phase de collision. La simulation progresse dans une alternance entre la collision et la propagation des particules.

Le développement et l'usage de ces méthodes connaissent une importante progression pour des géométries complexes cependant peu de travaux sont consacrés à la transition vers le régime instationnaire pour qualifier la capacité de ces méthodes à décrire la brisure de symétrie dans des écoulements, ce qui peut avoir une pertinence dans de nombreux domaines appliqués.

* Corresponding author.
E-mail address: ganaoui@unilim.fr (M. El Ganaoui).

1631-0721/$ – see front matter
doi:10.1016/j.crme.2009.12.008

Cette note succède à une précédente où l'on a présenté une extension de l'approche LB à la prise en compte de la transition de phase solide/liquide ainsi que des validations pour les problèmes de pure convection pour $Pr = 0,71$ jusqu'à des nombres de Rayleigh de 10^6 (Semma et al., 2007) [10]. Par ailleurs les auteurs de [11] ont conduit une étude paramétrique pour $0,71 \leqslant Pr \leqslant 70$ et $Ra \leqslant 10^5$. Cependant le cas des faibles couplages dynamique–thermique (Pr faible) qui n'est pas abordé dans ces références est important sur le plan fondamental et appliqué (notamment pour le contrôle des écoulements connaissant une brisure de symétrie).

On se focalise dans le présent contexte sur la perte de symétrie dans deux configurations sélectionnées pour leur importance pratique, les deux concernent des bains fondus métallique ($Pr \approx 10^{-2}$) qui représentent les configurations de base de croissance dirigée (partie fluide des dites ampoules de croissance). Le premier concerne la cavité horizontale (Horizontal Bridgman) à parois horizontales rigides et le second cas la cavité 2D chauffée par le bas à un quart supérieur adiabatique (Vertical Bridgman). Les deux largement considérées comme test des méthodes numériques de haute performance qui détaillent les scénarios de transition [19,23].

Pour la cavité horizontale (Fig. 2) l'écoulement décrit par gaz sur réseaux subit une brisure de symétrie pour $Gr_c = 32\,000$ (Fig. 4). La valeur obtenue par Volumes Finis est identifiée entre 32 500 et 33 500 (Gelfgat et al., 1999) [27] et par une méthode spectrale de haute précision elle est de 33 300 [22], soit un écart n'excédant pas 4% (Tableau 1).

Pour la cavité verticale (Fig. 3) l'écoulement décrit par gaz sur réseaux subit une brisure de symétrie pour $Gr_c = 275\,000$ (Fig. 5). La valeur par une approche VF étant de 350 000 [24], cette valeur est identifiée pour une méthode spectrale entre 250 000 et 300 000 [25], voir Tableau 2.

Par ailleurs les multiples solutions identifiées par l'approche gaz sur réseau sont également en bon accord avec les résultats de référence en présence d'un champ magnétique (Figs. 6 et 7).

Ainsi la méthode proposée traduit dans ces deux situations différentes une bonne prise en charge de la physique de la perte de symétrie de l'écoulement, ce qui est un premier pas dans l'analyse de la route vers le chaos de ce type d'écoulements. L'intérêt de montrer le traitement de ce type de problèmes liés à la croissance cristalline dirigée par des méthodes de type LB réside également dans une perspective de son extension à la prise en compte de la morphologie d'interface dans un calcul global (solide, liquide et interface de changement de phase) ce qui est plus coûteux en terme de mise en œuvre par une approche classique.

1. Introduction

The lattice Boltzmann (LB) method was proposed a decade and has been developed to simulate linear and nonlinear partial differential equations (such as wave motion equation, Burgers' equation, KdV equation and Lorenz equations) to offer progressively an alternative numerical method to traditional Computational Fluid Dynamics (CFD) for simulating fluid flows [1–11]. Unlike conventional methods based on a macroscopic continuum equation, the LB method starts from mesoscopic kinetic equation, i.e., the Boltzmann equation, to determine macroscopic fluid dynamics.

The kinetic nature brings certain advantages over conventional numerical methods, as parallel computation, and easy handling of complex geometries. The LBM has the beneficial feature of simulating classical flows, complex fluid flows such as multiphase flows, porous media flows, flows of suspensions, and compressible flows [5,10].

For instance, the method should be easier and intuitive to treat particular conditions like presence of obstacles. Moreover, the successive repetition of collisions and of propagations with LB approach allows an easy computer implementation.

In a preceding note [10], the developed scheme was applied to the classical natural convection in a square cavity and a good agreement was found by using traditional finite volume method for $Pr = 0.71$ and Ra increased until 10^6. Other works have been considered for $0.71 \leqslant Pr \leqslant 70$ and $Ra \leqslant 10^5$ [11]. However small Prandtl number liquids are for practical interest but not considered in those cited papers. The present work focuses on low Prandtl number fluid melts subject to symmetry breaking and transition to unsteady regimes. These configurations are for practical interest in crystal growth industry [12].

The interest of the LB treatment of such problem is also the perspective of coupling with the interface morphology serving global calculation including both macroscopic and microscopic interactions neighbouring the solid/liquid transition zone in the vicinity of the dendrites.

2. Model equations

It is important to reminder macroscopic equations before introducing LB method for simulating heat and fluid flow problems. The following paragraph describes the Partial Differential Equations (PDE) issue from the continuum medium approach.

2.1. Solution based on continuum medium formulation

Classically, the balance equations are derived from continuum media theory to describe transfers of mass, momentum and energy (and eventually species). The problem for natural convection consists to found P, $\mathbf{V}$ and T fields solution of the coupled PDE set:

$$\nabla \cdot \mathbf{V} = 0 \tag{1}$$

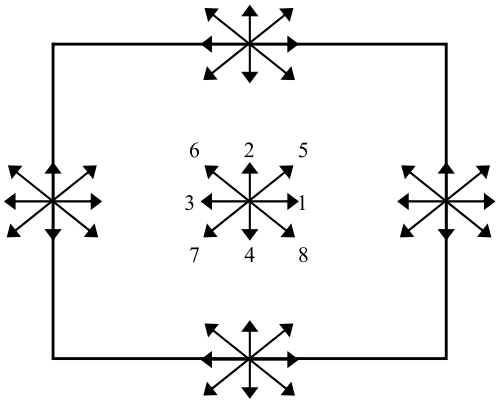

Fig. 1. Example of lattice grid (D2Q9).

Fig. 1. Exemple d'une grille de réseau (D2Q9).

$$\frac{\partial \mathbf{V}}{\partial t} + (\mathbf{V}\cdot\nabla)\mathbf{V} = -\nabla P + \nu\nabla^2\mathbf{V} - g\beta(T - T_0) \tag{2}$$

$$\frac{\partial T}{\partial t} + \mathbf{V}\cdot(\nabla T) = \chi\nabla^2 T \tag{3}$$

where $\mathbf{V}$ is the velocity vector, P is the pressure, ν and χ are the kinetic viscosity and thermal diffusivity respectively with assuming constant properties (ν, χ) and Boussinesq approximation for density ρ.

Numerical solution is ensured by using a 2nd-order finite volume method. Some variable may present a weak solution behaviour requiring the use of stable and less diffusive ULTRA–QUICK scheme associating a convective decentred quadratic scheme and a flux limitation strategy [13].

2.2. Solution based on lattice Boltzmann method

The well-known Boltzmann equation takes the following form:

$$\frac{\partial f}{\partial t} + \xi\cdot\nabla_x f + a\cdot\nabla_\xi f = \Omega(f, f) \tag{4}$$

where $f = f(x, \xi, t)$, a and Ω are the single particle distribution function, the body force and the collision term; x, ξ and t denote position, velocity and time, respectively.

The complicated collision term makes the Boltzmann equation difficult to solve. After the popular BGK (Bhatnagar–Gross–Krook) and Welander's approximations leading to BGKW [1], the collision term is well simplified and takes the new form:

$$\Omega_{BGK} = -\frac{1}{\lambda}\left(f - f^{eq}\right) \tag{5}$$

where λ is a typical time scale associated with collisional relaxation to the local equilibrium.

The exploitable discrete form of the lattice Boltzmann equation, after introducing BGKW approximation, becomes:

$$f_\alpha(x + e_\alpha\Delta t, t + \Delta t) - f_\alpha(x, t) = -\frac{1}{\tau_\nu}\left(f_\alpha(x, t) - f_\alpha^{eq}(x, t)\right) + e_\alpha\Delta t\cdot F_\alpha \tag{6}$$

where F_α is the external body force in the direction of the lattice discrete velocity e_α, $\tau_\nu = \lambda/\Delta t$, and f_α^{eq} is the equilibrium distribution function.

The philosophy of discrete velocity defines a terminology to the LB equation that is the lattices and arrangements noted as DnQm (n and m representing respectively the dimension of the problem and number of streaming direction). In the case of our two-dimensional problem, the D2Q9 square lattice is used (Fig. 1). The nine discrete velocities defined as:

$$e_\alpha = \begin{cases} (0, 0), & \alpha = 0 \\ (\cos[(\alpha-1)\pi/2], \sin[(\alpha-1)\pi/2]), & \alpha = 1, 2, 3, 4 \\ (\cos[(\alpha-5)\pi/2 + \pi/4], \sin[(\alpha-5)\pi/2 + \pi/4])\sqrt{2}c, & \alpha = 5, 6, 7, 8 \end{cases} \tag{7}$$

and the equilibrium distribution function:

$$f_\alpha^{eq} = \omega_\alpha\rho\left[1 + 3\frac{\vec{e}_\alpha\cdot\vec{V}}{c^2} + \frac{9}{2}\frac{(\vec{e}_\alpha\cdot\vec{V})^2}{c^4} - \frac{3}{2}\frac{\vec{V}^2}{c^4}\right] \tag{8}$$

where $w_0 = 4/9$, $w_\alpha = 1/9$ for $\alpha = 1, 2, 3, 4$, $w_\alpha = 1/36$ for $\alpha = 5, 6, 7, 8$ are weight factors, $c = \Delta x/\Delta t$ ($\Delta x = \Delta t = 1$ in LBM) is the lattice streaming velocity and $\vec{V} = (u, v)$.

The macroscopic fields, density and velocity, are computed by using the zero'th and first momentum of the density distribution function as follows:

$$\rho = \sum_\alpha f_\alpha$$
$$\rho \vec{V} = \sum_\alpha \vec{e}_\alpha f_\alpha \tag{9}$$

2.3. Recovering macroscopic equations

In this section we will summarise the way the LBGK model recovers the macroscopic quantities, such continuity and Navier–Stokes equations in their incompressible forms through the originally Chapman–Enskog multi-scale expansion technique, and under the assumption of low Mach number.

First, two macroscopic time scales $t_1 = \varepsilon t$ and $t_2 = \varepsilon^2 t$ and a macroscopic length scale $x_1 = \varepsilon x$, thus

$$\frac{\partial}{\partial t} = \varepsilon \frac{\partial}{\partial t_1} + \varepsilon^2 \frac{\partial}{\partial t_2} \quad \text{and} \quad \nabla = \varepsilon \nabla_1 \tag{10}$$

The Taylor expansion in time and space of Eq. (6) without forcing term can be written as:

$$D_\alpha f_\alpha + \frac{\Delta t}{2} D_\alpha^2 f_\alpha + O\left(\Delta t^2\right) = -\frac{1}{\tau \Delta t}\left(f_\alpha - f_\alpha^0\right) \tag{11}$$

where

$$D_\alpha = \frac{\partial}{\partial t} + c_\alpha \nabla = \varepsilon\left(\frac{\partial}{\partial t_1} + c_\alpha \nabla_1\right) + \varepsilon^2 \frac{\partial}{\partial t_2}$$

The expansion of f_α yields

$$f_\alpha = f_\alpha^{(0)} + \varepsilon f_\alpha^{(1)} + \varepsilon^2 f_\alpha^{(2)} + \cdots \tag{12}$$

where $f_\alpha^{eq} = f_\alpha^{(0)}$ and ε is a small parameter (Knudsen number) and the non-equilibrium part of the distribution function is $f_\alpha^{neq} = \varepsilon f_\alpha^{(1)} + \varepsilon^2 f_\alpha^{(2)} + \cdots$, then the constraints $\sum_\alpha f_\alpha^{(k)} = 0$ ($k \geqslant 1$) can be derived from Eqs. (8) and (11). Substituting Eqs. (10) and (12) in Eq. (11) and collecting the term of order ε and ε^2 gives:

$$D_{1,\alpha} f_\alpha^{(0)} = -\frac{f_\alpha^{(1)}}{\tau \Delta t} \tag{13}$$
$$\frac{\partial f_\alpha^{(0)}}{\partial t_2} + D_{1,\alpha} f_\alpha^{(1)} + \frac{\Delta t}{2} D_{2,\alpha} f_\alpha^{(0)} = -\frac{f_\alpha^{(2)}}{\tau \Delta t} \tag{14}$$

By the help of Eq. (13) we rewrite Eq. (14) as

$$\frac{\partial f_\alpha^{(0)}}{\partial t_2} + \left(1 - \frac{1}{2\tau}\right) D_{1,\alpha} f_\alpha^{(1)} = -\frac{f_\alpha^{(2)}}{\tau \Delta t} \tag{15}$$

By taking summation, over the index α, of zero'th-order moment of Eqs. (13) and (15) we obtain

$$\frac{\partial \rho}{\partial t_1} + \nabla_1(\rho \vec{V}) = 0 \tag{16}$$
$$\frac{\partial \rho}{\partial t_2} = 0 \tag{17}$$

Then multiplying Eq. (16) by ε and (17) by ε^2 and summing gives the continuity equation

$$\varepsilon \frac{\partial \rho}{\partial t_1} + \varepsilon^2 \frac{\partial \rho}{\partial t_2} + \varepsilon \nabla_1(\rho \vec{V}) = \frac{\partial \rho}{\partial t} + \nabla(\rho \vec{V}) = 0 \tag{18}$$

By taking summation, over the index α, of first order moment of Eqs. (13) and (14) we obtain

$$\frac{\partial(\rho V_i)}{\partial t_1} + \nabla_1 \prod_{ij}^{(0)} = 0 \tag{19}$$

$$\frac{\partial(\rho V_i)}{\partial t_2} + \left(1 - \frac{1}{2\tau}\right)\nabla_1 \sum_{\alpha=1}^{9} \vec{c}_{\alpha i}\vec{c}_{\alpha j} f_\alpha^{(1)} = 0 \tag{20}$$

$$\sum_{\alpha} \vec{c}_{\alpha i}\vec{c}_{\alpha j} f_\alpha^{(1)} = \sum_{\alpha=1}^{9} \vec{c}_{\alpha i}\vec{c}_{\alpha j}(-\tau\,\Delta t) D_{\alpha 1} f_\alpha^{(0)} = -\tau\,\Delta t \sum_{\alpha=1}^{9}\left(\frac{\partial}{\partial t}\prod_{ij}^{(0)} + \nabla_1 \prod_{ij}^{(1)}\right) \tag{21}$$

where

$$\prod_{ij}^{(0)} = \sum_{\alpha=1}^{9} \vec{c}_{\alpha i}\vec{c}_{\alpha j} f_\alpha^{(0)} = \rho V_i V_j + \rho c_s^2 I$$

and

$$\prod_{ij}^{(1)} = \sum_{\alpha=1}^{9} \vec{c}_{\alpha i}\vec{c}_{\alpha j}\vec{c}_{\alpha k} f_\alpha^{(0)} = \rho c_s^2(\delta_{ij}V_k + \delta_{jk}V_i + \delta_{ki}V_j)$$

thus, Eq. (19) can be written as

$$\frac{\partial(\rho V_i)}{\partial t_1} + \nabla_1\left(\rho V_i V_j + \rho c_s^2 I\right) = 0 \tag{22}$$

and after neglecting terms of order of $O(Ma^2)$, Eq. (20) becomes

$$\frac{\partial(\rho V_i)}{\partial t_2} - \left(\tau - \frac{1}{2}\right)c_s^2 \Delta t \nabla_1^2(\rho V_i) = O\left(\varepsilon + Ma^2\right) \tag{23}$$

By multiplying Eq. (22) by ε and Eq. (23) by ε^2 and summing yields to the Navier–Stokes equations

$$\frac{\partial V_i}{\partial t} + \nabla(V_i V_j) = \frac{\nabla P}{\rho} + \nu\nabla^2 V_i + O\left(\varepsilon^2 + \varepsilon Ma^2\right) \tag{24}$$

Then a pressure defined as $P = \rho c_s^2$ where $c_s = c/\sqrt{3}$ is the sound speed and the kinetic viscosity becomes $\nu = (\tau_\nu - \frac{1}{2})c_s^2\Delta t$.

It is important to note here that Eqs. (16) and (22) form the Euler equations.

2.4. Developing of the thermal model

Since thermal flows are always encountered, a thermal model (IEDDF) was proposed, which overcomes the difficulty of fixed Prandtl number and based on the idea of new distribution function to evaluate the internal energy. A coupled model is developed in [14], it has the feature of using two independent lattices. Y. Peng et al. (2003) [3] use the fact that the compression work done by the pressure and the viscous heat dissipation can be neglected in incompressible flows, and then simplify the IEDDF. The new form saves the standard form of LBM and does not have gradient terms.

The evolution equation of the new thermal model is defined as:

$$g_\alpha(\vec{x} + \vec{e}_\alpha\delta t, t + \delta t) - g_\alpha(\vec{x}, t) = -\frac{\delta t}{\tau_\chi}\left[g_\alpha(\vec{x}, t) - g_\alpha^{eq}(\vec{x}, t)\right] \tag{25}$$

where the thermal diffusivity is defined as $\chi = (2\tau_\chi - 1)c_s^2\Delta t$.

The correspondent equilibrium energy distribution function following the work of [3] is defined as:

$$g_\alpha^{eq} = \omega_\alpha \rho\varepsilon\left[\frac{3(\vec{c}_\alpha^2 - \vec{V}^2)}{2c^2} + 3\left(\frac{3\vec{c}_\alpha^2}{2c^2} - 1\right)\frac{(\vec{c}_\alpha\cdot\vec{V})}{c^2} + \frac{9}{2}\frac{(\vec{c}_\alpha\cdot\vec{V})^2}{c^4}\right] \tag{26}$$

where $\varepsilon = DRT/2$ ($D = 2$, $R = 1$ in LBM), then the macroscopic temperature is computed from:

$$\rho\varepsilon = \sum_{\alpha} g_\alpha \tag{27}$$

2.5. Boundary conditions in LBM

Implementation of boundary conditions is an essential issue in LBM. In this model the bounce-back rule of the non-equilibrium distribution function proposed in [3] is used for the Dirichlet type boundary condition. The density distribution function at the boundary should satisfy:

$$f_\alpha^{neq} = f_\beta^{neq} \tag{28}$$

The energy distribution function at the boundary satisfies:

$$g_\alpha^{neq} - \vec{c}_\alpha^2 f_\alpha^{neq} = -\left(g_\beta^{neq} - \vec{c}_\beta^2 f_\beta^{neq}\right) \tag{29}$$

where $\vec{c}_\alpha$ and $\vec{c}_\beta$ have opposite directions.

Since the distribution functions that point out of the fluid fields are determined by the streaming process, we have only to specify the distribution functions that point into the fluid field at a given boundary node. At the top wall of a wall boundary condition kind (see Fig. 1) the distributions at directions 1, 2, 3, 5, and 6 are known and are computed through Eq. (6). The unknown distributions at directions 4, 7 and 8 can be determined by the boundary conditions of Eq. (28) as

$$f_4 = f_4^{eq} + f_2 - f_2^{eq}, \qquad f_7 = f_7^{eq} + f_5 - f_5^{eq} \quad \text{and} \quad f_8 = f_8^{eq} + f_6 - f_6^{eq}$$

For the Neumann type boundary condition is transferred to Dirichlet type condition by the common used relation in order to get the temperature at the given wall node. That relation is expressed as:

$$T_{0,wall} = \frac{4T_1 - T_2}{3} \tag{30}$$

It is worth noting that the well-known natural convection velocity scale $U_0 = (g\beta\Delta T H)^{0.5}$ $(H \equiv m)$ will be adopted to ensure the incompressible condition $(Ma = U_0/c_s < 0.15)$. From this condition and (ν, χ) definitions the Prandtl number is calculated as $Pr = \frac{\nu}{\chi} = \frac{\tau_\nu - 0.5}{2\tau_\chi - 1}$ and the Rayleigh number is adjusted as $Ra = \frac{g\beta\Delta T H^3}{\nu\chi} = \frac{U_0^2}{Pr}(\frac{H}{\chi})^2$; then the length scale $H \equiv m$ obeys the condition $H > \frac{\chi}{Ma}(\frac{Ra}{Pr})^{0.5}$.

3. Results and discussion

Let first mention that some validations have been made regarding commonly used test cases of natural convection in a square cavity [15]. Prandtl number is fixed to $Pr = 0.71$ and Rayleigh number is varied between 10^3 and 10^6. LB solution is carried out by using the particle velocity model referred as D2Q9 grid (Fig. 1). Good agreement is found between LB results and classical based Navier–Stokes simulations [9,10]. The little difference with the reference results (within 1%) can be considered acceptable for engineering application. Here the validation is extended to symmetry breaking in low Prandtl number flows.

3.1. Transitional test cases definition

In recent years, there has been a growing interest in studying liquid metal flows in solidification cavities as an academic useful configuration for process of solidification. Such technique remains today an interesting field of several numerical and fundamental works and leading to specific numerical and experimental benchmarks [16].

When the fluid is heated from below, the flow exhibits a very strong and complex nonlinear behaviour [17–21]. The variety of related Rayleigh–Bénard (RB) problems offer a first approach to understand the flow/transfers complexity evolving from a conductive solution to a convective one.

Let consider two kinds of configurations both used as a typical enclosure for fluid flowing for solidification (Bridgman growth). The understanding of heat and mass transfer in crystal growth technique has become an important subject, this because of producing single crystals is the problem of modern technology. The studied problem focuses on stability diagrams.

For the terminology, SS–SAS (resp. SAS–P1) means a transition from steady symmetric (SS) regime to steady asymmetric (SAS) one (resp. from steady asymmetric (SAS) regime to mono-periodic one (P1)).

For the case 1 the problem is as depicted in Fig. 2(a), the melt is heated from left and cooled from the right (crystal-side). The width of the melt is defined by the interface-shape. Since the most benchmarks available in literature take the case of fixed interface, we will adopt such simplified configuration for purpose of comparison as zoomed in Fig. 2(b). The computational domain is then a rectangular cavity $[0, L] \times [0, H]$ of aspect ratio $A = L/H = 4$ filled with a fluid of $Pr = 0.015$. The left and right walls are maintained at constant temperatures while the top and bottom walls are adiabatic $T(0, y) = T_H$ and $T(L, y) = T_C < T_H$.

For the case 2, Fig. 3 illustrates the geometry of the enclosure filled with gallium $(Pr = 0.01)$. The upper mid-part is cooled so this is the solid phase, the lower mid-part is heated and so it is the molten phase. At the mid-height, the

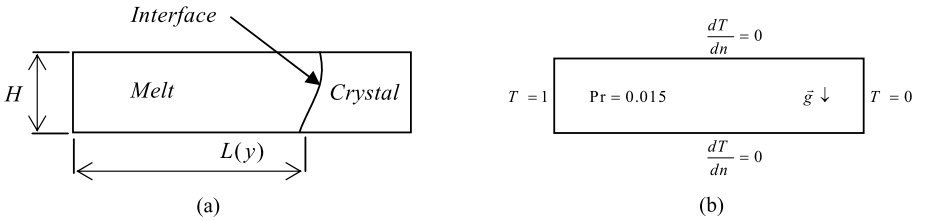

Fig. 2. Horizontal Bridgman melt-crystal growth (a) and a simplified configuration (b).

Fig. 2. Technique de Bridgman horizontale (a) et configuration simplifiée (b).

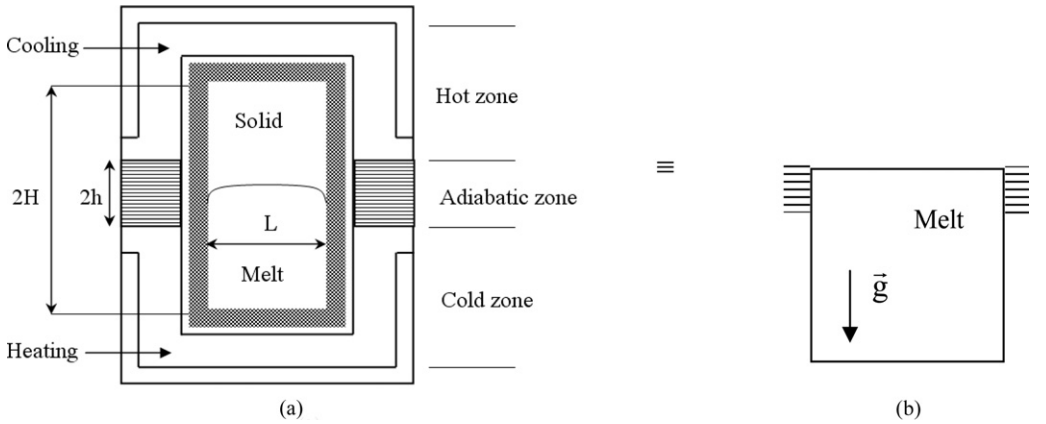

Fig. 3. Vertical Bridgman melt growth (a) and simplified configuration (b).

Fig. 3. Technique de Bridgman verticale (a) et configuration simplifiée (b).

enclosure is insulated along a height $2h$. The remaining parts of the right and left boundaries are heated-up to a height $3H/4$. The investigated cases correspond to $L = H$ and $h = H/4$, the cavity is thus called quarter insulated, cooled at the top and heated from below and is presently subject to tridimensional simulation [20,21]. The fluid flow is subjected to the action of gravity. The resolution taken for all performed calculations is 100^2.

For the nondimensionalization we use the scales H, H^2/α, α/H and $\rho(\alpha/H)^2$ (α is the thermal diffusivity) for length, time, velocity and pressure respectively and $\theta = (T - T_r)/(T_h - T_c)$ is the dimensionless temperature, where T_r is a temperature reference resulting on the Grashof number $Gr = g\beta\Delta T H^3/\alpha^2$, and the Prandtl number $Pr = \nu/\alpha$ and Hartmann number $Ha = B_0 H/(\mu_0\lambda\rho\nu)^{1/2}$ (μ_0 is the magnetic permeability and λ is the magnetic diffusivity for a characteristic magnetic field B_0).

3.2. Case test 1: routes to unsteadiness in the horizontal Bridgman model

To compare to available literature finding results are presented in terms of Grashof number based on the height of the cavity.

This regime exhibits the Hopf bifurcation followed by an instable regime sensitive to Gr variations. Another stable branch is also identified showing two-cell solution.

The resolution for present calculations is taken 400×100. The comparison is made with the well-established benchmark problem and diagram of stability. The author uses two independent methods (finite volume methods) and compares his results with high accuracy numerical solutions (spectral methods) in former works of [22,23].

For $Gr = 5 \times 10^3$, the flow is a one convective clock-wise rotating cell. With increasing the Gr, the flow structure undergoes a distortion to a strict change: the flow structure is a structure of three counter-rotating cells. This transition occurs at a critical value $Gr \approx 32\,000$. The present results are summarised together with the previous solutions in Table 1. The bifurcation diagram is defined by the plot of maximum stream-function magnitude vs the Grashof number (Fig. 4). In the vicinity of this critical point the Grashof number is increased uniformly (by a step of 250). For $Gr = 32\,250$, the flow exhibits a three-cell structure (Fig. 4(e)). For $Gr = 32\,500$, a new transition is identified: the flow becomes two-cell structure. The regime remains steady again with two rolls until $Gr = 33\,330$, moreover we choose to perform a calculation for $Gr = 40\,000$, a change in the cell-shape is observed (see Fig. 4(f)), the stream-function magnitude increases considerably and no time dependency is remarked. This behaviour defines a new branch with two cells in the flow patterns which have been more studied in [22–24].

Table 1
Present LB results versus the literature results, $A = 1$ and $Pr = 0.71$.

Tableau 1
Résultats LB comparés à la littérature, $A = 1$ et $Pr = 0.71$.

Method	Stretched finite difference (FD) (Ben Hadid et al., 1990)	Chebyshev spectral (Pulicanni et al., 1990)	Biquadratic finites elements (FE) (Winter, 1988, 1990)	Uniform finite volumes (FV) (Gelfgat et al., 1999)	Global Galerkin method (Gelfgat et al., 1999)	LBM (present result)
Mesh	121×41	40×30	66×24	60×24	200×100	400×100
Gr	32 500–33 500	33 300	33 002	32 500–33 500	32 996	32 000

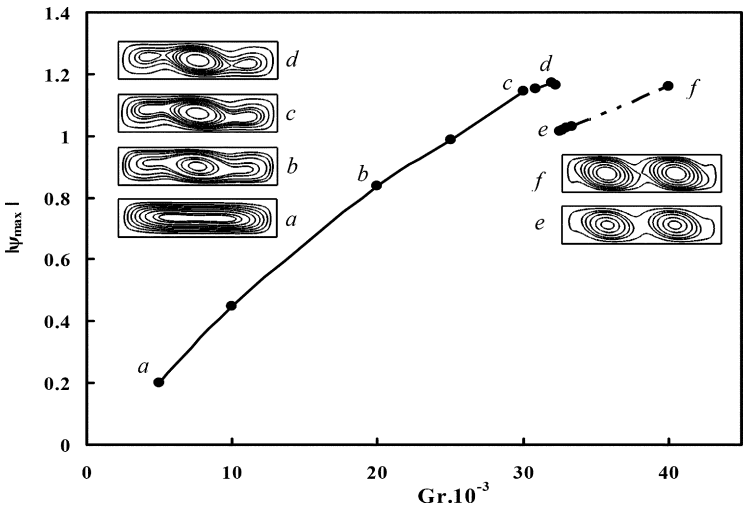

Fig. 4. Bifurcation diagram for the horizontal Bridgman (fixed interface model) for $Pr = 0.015$.
Fig. 4. Diagramme de bifurcation pour le modèle horizontal (à interface fixe) $Pr = 0.015$.

For the heat transfer, the left Nusselt number is about 0.255 for $Gr = 5000$, it increases notably to reach 0.287 for $Gr = 20\,000$ and remains almost constant until $Gr = 32\,500$. For $Gr = 32\,500$, we have a two-cell flow leading to a little decrease in the left Nusselt number (0.281).

The left cell turns the heated fluid (coming from the upper-left corner) before it will be cooled by the cold wall. Thus, it will be a small temperature difference at the hot wall. Increasing the Grashof number to 40 000 enhances the convection phenomenon (the Nusselt number increases more to 0.297).

One can observe that results of this LB model go well with those of previous works and LBM can predict accurately the threshold of transition in horizontal Bridgman growth as the traditional methods in CFD which almost of them situate the Gr_c between 32 500 and 33 500.

3.3. Case test 2: routes to unsteadiness in the vertical Bridgman model

The cavity heated from below (Fig. 3), is characterised by a typical symmetry breaking in the melt flow structure from the earlier Grashof numbers. Indeed for $Gr = 10^5$ that corresponds to low values of the Rayleigh number ($Ra = Gr\,Pr = 10^3$), the flow is a steady symmetric structure characterised by two counter-rotating cells. Since the thermal transfer is enhanced by increasing *Gr*, the flow becomes slightly asymmetric for $Gr = 25 \times 10^4$. The stream-function magnitude follows the increase of the Grashof number, to achieve 0.3786 (for $Gr = 25 \times 10^4$). While for $Gr = 3 \times 10^5$, its value is of 0.3517, then a maximum in stream-function magnitude is reached between 25×10^4 and 3×10^5. This critical value is about $Gr_c \approx 27.5 \times 10^4$ (see Fig. 5) and indicates a change in the flow pattern expressed by a symmetry breaking (SS–SAS). This behaviour confirmed by the 2D studies of [25] where transition threshold is identified between 25×10^4 and 3×10^5 using spectral method. The result goes also well with recent 3D solutions of [20,21]. A comparative table recapitulates each result gathered to the used method (see Table 2).

The diagram of Fig. 5 illustrates the response by increasing more the *Gr*. For $Gr = 3 \times 10^5$ (c), the steady flow is absolutely asymmetric and we observe the growth of the left roll and the reduction of the right one. For $Gr = 6 \times 10^5$, the flow structure is completely different, the whole domain is dominated by one roll slightly distorted by the presence of the small two left vortices and the two linked right vortices that will be defeated for $Gr = 10^6$.

The flow remains steady with four vortices at the corners and one dominate cell formed by perfect circles centred at the cavity centre until $Gr = 17 \times 10^5$. Next tested values of *Gr* (17.5×10^5 and 17.75×10^3) give an unsteady state (SAS–P1).

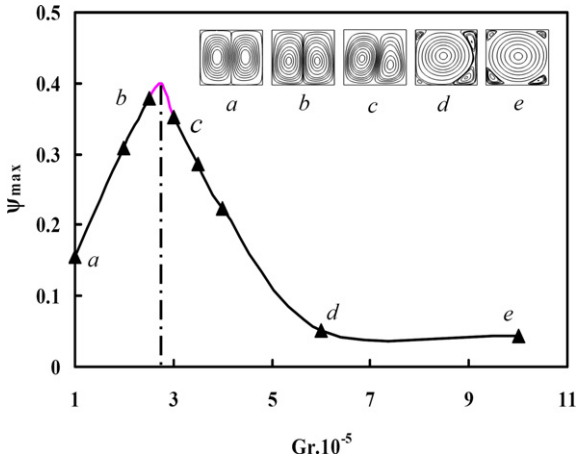

Fig. 5. Threshold transition diagram for the vertical Bridgman model (fixed interface) for $Pr = 0.01$.

Fig. 5. Diagramme de bifurcation pour le modèle de Bridgman vertical (à interface fixe) $Pr = 0.01$.

Table 2
Symmetry breaking, Hopf point estimate with various methods for fixed interface, $A = 4$ and $Pr = 0.015$.

Tableau 2
Brisure de symétrie, estimation du point de bifurcation de Hopf avec différentes méthodes, $A = 4$ et $Pr = 0.015$.

Method	Symmetric $Gr = 20 \times 10^4$ Ψ_{max}	Transition SS–SAS Gr	Transition SAS–P1 Gr(frequency)
Spectral (P. Larroudé et al., 1994)	–	25×10^4–30×10^4	200×10^4
FV (2D) (Semma, 2004)	0.290	35×10^4	175×10^4 $f = 6.67$
FV (3D) (Bennacer et al., 2006)	–	30×10^4	–
LBM (present)	0.308	27.5×10^4	179×10^4 $f = 7.033$

The stream-function magnitude decreases more and the flow becomes periodic for $Gr = 17.9 \times 10^5$, with a dimensionless frequency $f_c = 7.033$. The deviation from the FV's results ($f_c = 6.67$) obtained in [25] is about 5.44%, this can be attributed to the sum errors of the first accurate approximation in the collision term in Eq. (5) and the deviation (in order of Ma^2) in recovering macroscopic quantities in Eqs. (18) and (24).

It is well to mention that the grid-independency has been checked by performing a calculation using 200^2 grid-size and no significantly effects on Gr_c or f_c were observed.

One can see that our results are close to the spectral ones and the two results are close to the 2d and 3d finite volume ones.

3.4. Solution multiplicity in a horizontal Bridgman model under uniform magnetic field

The objective of this section is to extend the LBM to study the solution multiplicity problems in flows under magnetic field [26–28]. To our knowledge, it is the first attempt of LBM to transitional flows. The LBM algorithm is applied to the horizontal Bridgman model flow (test case 1) subjected to a uniform magnetic field. The magnetic field takes several inclinations ϕ. The simple lattice Boltzmann form in Eq. (6) is not available for body force including spatial and temporal variation (such as electromagnetic force). Further reading can be found in [29] for the most suitable form taking account the body force and in [27] and [28] for implementation and assumptions. Then, rigorous test of the present LBM will be given for several Hartmann numbers ($0 \leqslant Ha \leqslant 20$) and inclination angle ($0 \leqslant \phi \leqslant 90$) for a Grashof number ($1 \times 10^5 \leqslant Gr \leqslant 6 \times 10^6$).

A quantitative test is presented, at first, to check the model correctness: $Ha = 20$, $\phi = 0$ and $Gr = 5.4 \times 10^6$. The flow state is found to be periodic. The averaged Nusselt number is 3.6052, the maximum stream function magnitude is 371.6046 and the flow frequency is 3.32×10^{-3}. The correspondent values in [27] are 3.4377, 365.948 and 3.26×10^{-3} respectively.

Furthermore, the qualitative comparison in Fig. 6 shows a good agreement between our results for $Gr = 5.4 \times 10^6$ and those of [27].

Now we examine the dependence of critical Grashof number (of transition from steady one-cell flow) on Hartman number and the magnetic field orientation. The calculations are performed for different Ha and for inclinations $\phi = 0°$, $45°$ and $90°$. The grid size is taken 120×480 for all computations. The results are summarised in the stability diagram of Fig. 7.

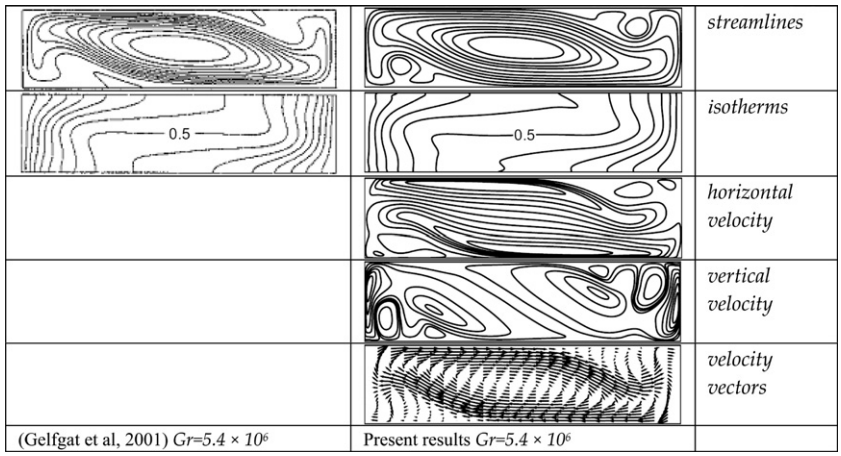

Fig. 6. Comparisons of present and literature results for solution multiplicity in presence of a magnetic field.

Fig. 6. Comparaisons entre les résultats du présent travail et ceux de la littérature dans le cas de solutions multiples en présence d'un champ magnétique.

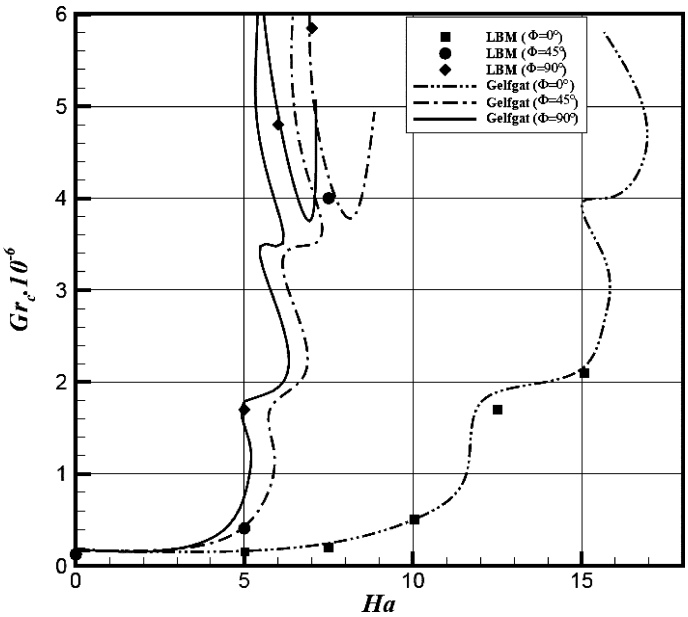

Fig. 7. Stability diagram for steady one-cell flow: dependence of critical Grashof number on Hartman number (*Ha*) and inclination of magnetic field. Lines: results in Gelfgat et al. [27]. Symbols: our predictions.

Fig. 7. Diagramme de stabilité pour le cas stationnaire (1 cellule) : dépendance du nombre de Grashof critique en *Ha* et en inclinaison du champ. Lignes : résultats de Gelfgat et al. [27]. Symbols : présentes prédictions.

It was found that for $\phi = 0°$, the electromagnetic force is $\boldsymbol{F} = \boldsymbol{F}_y = -\sigma B^2 v$, then, it counteracts the vertical velocity and a competition takes place (Fig. 6(e)) at mid-height near the vertical walls where the layers become more stretched, and increasing the Hartman number will increase Gr_c. The convective motion is the most pronounced near the horizontal walls (Fig. 6(e)). However, for $\phi = 90°$, the electromagnetic force is $\boldsymbol{F} = \boldsymbol{F}_x = -\sigma B^2 \boldsymbol{u}$, then, it counteracts the horizontal component of the velocity. The convective motion is, then, stabilised. The threshold transition will be delayed.

For general cases, the electromagnetic force is a function of the inclination ϕ and both horizontal and vertical components of velocity: $\boldsymbol{F} = \sigma B^2(v\sin(\phi)\cos(\phi) - u\sin^2(\phi), u\sin(\phi)\cos(\phi) - v\cos^2(\phi))$. The stability diagram (Fig. 7) shows that the Gr_c increases with increasing *Ha* or ϕ.

In the other hand, one can see that our LBM model gives precise prediction that compares well former work obtained using the global Galerkin method.

4. Conclusion

This Note provides an illustration of treating transition to unsteadiness and multiple solution problems by using a lattice Boltzmann approach for flows coupled to heat transfer.

The main concern in this work is focusing on the prediction of the transition thresholds less concerned in the literature result devoted to the present interest to LBM. The main published work at the best of our knowledge is focusing of steady solution or fully unsteady flows.

Then the paper focused on the accuracy of the method to identify transitional thresholds. It has been chosen to focus here on the symmetry breaking and first transition to unsteady regime. Both horizontal and vertical enclosures are considered and the results are in good agreement with accurate literature values for transitional thresholds in considered configurations. The work follows on providing an analysis of unsteady flows becoming periodic and chaotic especially in enclosures interesting directional solidification. In such configuration it is important to describe accurately complex fluid flow and interface deformations.

The LB method offers the advantage that such scheme can easily be extended to consider the interface morphology, local micro-flows and local solidification structures leading on developing global simulation codes coupling micro/macro aspect in 3D configuration and straightforwardly implemented on machines.

By the way this work is a step ahead on unsteadiness investigations to consider rapid and multiscales phenomena as in turbulent flow simulation.

Acknowledgements

Authors would like to express their gratitude to professors Abdumajeed Mohamad from the University of Calgary for fruitful discussions on LB methods during his visits to the University of Limoges (CNRS SPCTS Lab.).

References

[1] A.A. Mohamad, Applied Lattice Boltzmann Method for Transport Phenomena, Momentum, Heat and Mass Transfer, 2007.
[2] M. Bouzidi, D. d'Humières, P. Lallemand, L.-S. Luo, Lattice Boltzmann equation on a two-dimensional rectangular grid, Journal of Computational Physics 172 (2001) 704–717.
[3] Y. Peng, C. Shu, Y.T. Chew, Simplified thermal lattice Boltzmann model for incompressible thermal flows, Physical Review E 68 (2003) 026701.
[4] J.I.D. Alexander, S. Chen, J.D. Sterling, Lattice Boltzmann thermohydrodynamics, Physical Review E 47 (1993) R2249.
[5] M. Jami, A. Mezrhab, M. Bouzidi, P. Lallemand, Lattice-Boltzmann computation of natural convection in a partitioned enclosure with inclined partitions attached to its hot wall, Physica A: Statistical Mechanics and Its Applications 368 (2) (2006) 481–494.
[6] R. Djebali, M. El Ganaoui, H. Sammouda, Investigation of a side wall heated cavity by using lattice Boltzmann method, Revue Europeenne de Mecanique Numérique (REMN) 18 (2) (2009) 217–238.
[7] R. Djebali, M. El Ganaoui, H. Sammouda, R. Bennacer, Some benchmark solutions of a side wall heated cavity using lattice Boltzmann approach, Fluid Dynamics & Material Processing (FDMP) 164 (1) (2009) 1–21.
[8] A.A. Mohamad, M. El Ganaoui, R. Bennacer, Lattice Boltzmann simulation of natural convection in an open ended cavity, International Journal of Thermal Sciences (IJTS) 48 (10) (October 2009) 1870–1875.
[9] E. Semma, M. El Ganaoui, R. Bennacer, A.A. Mohamad, Investigation of flows in solidification by using the lattice Boltzmann method, International Journal of Thermal Sciences 47 (2008) 201–208.
[10] E.A. Semma, M. El Ganaoui, R. Bennacer, Lattice Boltzmann method for melting/solidification problems, Comptes Rendus Mécanique 335 (5–6) (May–June 2007) 295–303.
[11] P.-H. Kao, R.-J. Yang, Simulating oscillatory flows in Rayleigh–Bénard convection using the lattice Boltzmann method, International Journal of Heat and Mass Transfer 50 (2007) 3315–3328.
[12] G. Muller, G. Neumann, W. Weber, Natural convection in vertical Bridgman configuration, Journal of Crystal Growth 70 (1984) 78–93.
[13] A. Semma, M. El Ganaoui, A. Cheddadi, A. Farchi, High order finite volume scheme for phase change problems, in: F. Benkhaldoun, D. Ouazar, S. Raghay (Eds.), Finite Volumes for Complex Applications, vol. IV, Hermès Science Publishing, 2005, pp. 493–503.
[14] X. He, S. Chen, G.D. Doolen, A novel thermal model for the lattice Boltzmann method in incompressible limit, Journal of Computational Physics 146 (1998) 282–300.
[15] G. de Vahl Davis, Natural convection of air in a square cavity: A benchmark numerical solutions, International Journal of Numerical Methods in Fluids 3 (1983) 249–264.
[16] Xiao Dong Wang, Yves Fautrelle, An investigation of the influence of natural convection on tin solidification using a quasi two-dimensional experimental benchmark, International Journal of Heat and Mass Transfer 52 (23–24) (November 2009) 5624–5633.
[17] E. Semma, V. Timchenko, M. El Ganaoui, E. Leonardi, The effect of wall temperature fluctuations on the heat transfer and fluid flow occurring in a liquid enclosure, International Journal of Heat and Fluid Flow 26 (2005) 547–557.
[18] E.A. Semma, M. El Ganaoui, V. Timchenko, E. Leonardi, Some thermal modulation effects on directional solidification, Fluid Dynamics & Materials Processing (FDMP) 2 (3) (2006) 191–202.
[19] M. El Ganaoui, P. Bontoux, A homogenization method for solid–liquid phase change during directional solidification, HTD-vol. 361-5, in: Proceeding of the ASME Heat Transfer Division, vol. 5, ASME, 1998.
[20] R. Bennacer, M. El Ganaoui, E. Leonardi, Symmetry breaking of melt flow typically encountered in a Bridgman configuration heated from below, Applied Mathematical Modelling 30 (2006) 1249–1261.
[21] F. Mechighel, M. El Ganaoui, M. Kadja, B. Pateyron, S. Dost, Numerical simulation of three dimensional low Prandtl liquid flow in a parallelepiped cavity under an external magnetic field, Fluid Dynamics & Materials Processing (FDMP) 5 (4) (2009) 313–330.
[22] J.P. Pullicani, E.C. Del Arco, A. Randriamampianina, P. Bontoux, R. Peyret, Spectral simulations of oscillatory convection at low Prandtl number, International Journal of Numerical Methods in Fluids 10 (1990) 481.
[23] H. Zhou, A. Zebib, Oscillatory convection in solidifying pure metal, Numerical Heat Transfer, Part A 22 (1992) 435–468.
[24] A. Semma, Etude numérique des transferts de chaleur et de masse durant la croissance dirigée : effet de paramètres de contrôle, Thèse de doctorat de l'école Mohammadia d'Ingénieurs, Université Mohamed V, Maroc, 2004.

[25] P. Larroudé, J. Ouazzani, L.I.D. Alexander, P. Bontoux, Symmetry breaking flow transitions and oscillatory flows in a 2D directional solidification model, European Journal of Mechanics B 13 (3) (1994) 353–381.
[26] M. El Ganaoui, D. Morvan, P. Larroude, P. Bontoux, Numerical simulation of gravitational effects during directional solidification, Advances in Space Research 22 (8) (1998) 1175–1178.
[27] A.Yu. Gelfgat, P.Z. Bar-Yoseph, The effect of an external magnetic field on oscillatory instability of convective flows in a rectangular cavity, Physics of Fluids 13 (8) (2001) 2269–2278.
[28] M.C. Ece, E. Büyük, Natural-convection flow under a magnetic field in an inclined rectangular enclosure heated and cooled on adjacent walls, Fluid Dynamics Research 38 (2006) 564–590.
[29] Z. Guo, C. Zheng, B. Shi, Discrete lattice effects on the forcing term in the lattice Boltzmann method, Physical Review E 65 (2002) 046308.